

1 **A two-dimensional hydro-morphological model for river** 2 **hydraulics and morphology with vegetation**

3 Mingfu Guan^{1*}, Qihua Liang²

4 ¹ Department of Geography, Loughborough University, LE11 3TU, UK

5 ² School of Civil Engineering and Geosciences, Newcastle University, NE1 7RU, UK

6 * Corresponding to: mingfu.guan@hotmail.com

7 **ABSTRACT:** This work develops a two-dimensional (2D) hydro-morphological model which can
8 be used to simulate river hydraulics and morphology under the condition of various vegetation
9 covers. The model system consists of five modules, including a hydrodynamic model, a sediment
10 transport model, a vegetation model, a bank failure model and a bed deformation model. The
11 secondary flow effects are incorporated through additional dispersion terms. The core
12 components of the model system solve the full shallow water equations; this is coupled with a
13 non-equilibrium sediment transport model. The new integrated model system is validated against
14 a number of laboratory-scale test cases and then applied to a natural river. The satisfactory
15 simulation results confirm the model's capability in reproducing both stream hydraulics and
16 channel morphological changes with vegetation. Several hypothetical simulations indicate that
17 the model can be used not only to predict flooding and morphological evolution with vegetation,
18 but also to assess river restoration involving vegetation.

19 **KEYWORDS:** vegetation effects; non-equilibrium sediment transport model; river hydraulics;
20 morphological changes; shallow water equations

21

22 **1. Introduction**

23 Vegetation plays multiple roles in real-world river streams. For example, riparian vegetation can
24 protect against bank erosion, and in-stream vegetation may significantly influence flow
25 propagation, sediment movement and river morphology (Darby, 1999; Hickin, 1984; Hupp and
26 Osterkamp, 1996; Keller and Swanson, 1979). Vegetation has been widely used for improving

27 stream corridor habitat and other ecological functions in many river restoration programmes.
28 Understanding the multiple effects of vegetation is highly important in river management.

29 In the recent decades, the effects of vegetation on river flows have been extensively investigated
30 through laboratory experiments (Armanini et al., 2010; Bennett et al., 2008; Gorrick and
31 Rodríguez, 2012; Jordanova and James, 2003) and modelling (e.g. (Anderson et al., 2006;
32 Crosato and Saleh, 2011; Gran and Paola, 2001; Jang and Shimizu, 2007; Li and Millar, 2011;
33 Tal and Paola, 2007; Tal and Paola, 2010; Tsujimoto, 1999; Wu et al., 2005b)). These studies
34 have clearly emphasised that vegetation affects flow hydraulics in various ways, and thereby
35 plays a crucial role in river morphology and ecological diversity. However, the majority of the
36 existing studies have been focused on the effects of vegetation on pure flow characteristics, with
37 some considering the long-term flow-vegetation-sediment interaction in braided rivers. Research
38 into the direct fluvial response to vegetation during flooding remains rare.

39 On the other hand, numerical models for hydro-geomorphological processes have been
40 extensively developed (Guan et al., 2013; Guan et al., 2015b; Liang, 2010). When considering
41 the importance of vegetation, hydro-morphological modelling should take into account the
42 vegetation effects, particularly under conditions where vegetation may play a key role. Flow-
43 sediment-vegetation interaction is a highly complex process where the three components may
44 dynamically interact with each other. Few models have been reported to represent the whole
45 physical process. The current study, therefore, presents a hydro-morphodynamic model with the
46 inclusion of vegetation dynamics to fill this knowledge gap.

47 In reality, vegetation may or may not be fully submerged by river flows. For example, soft grass
48 and plants are generally submerged during flooding seasons, while rigid vegetation, e.g. trees is
49 usually emergent. In hydraulic and sediment transport modelling, the effects of vegetation is
50 conventionally taken into account through increased resistant force and the Manning's equation
51 has been the most widely-used approach to represent flow resistance (Green, 2005; Guan et al.,
52 2013; Guan et al., 2015b; Liang, 2010; Sellin et al., 2003; Wu et al., 1999). The Manning's
53 coefficient is usually estimated according to specific channel conditions and its accurate
54 estimation requires abundant experience. However, this traditional way of representing flow

55 resistance is not appropriate for cases when rigid plants are present, e.g. flow through emergent
56 vegetation. In such flow scenarios, resistance is primarily exerted by the stem's drag throughout
57 the flow depth rather than by shear stress at the bed (James et al., 2004). A more appropriate
58 approach is to split channel resistance into several components and then estimate each one
59 separately (Cowan, 1956; Morin et al., 2000). Recently, some approaches have been
60 successively proposed to estimate the flow resistance for modelling flows over or through a
61 vegetated channel (Baptist et al., 2007; Vionnet et al., 2004). This study adopts the estimation
62 method of separating the total resistance into vegetation resistance and bed resistance. The
63 vegetation resistance is then treated as a *drag force* exerted by vegetation. This vegetation
64 resistance usually dominates flow resistance for the vegetated flows (Temple, 1986; Wu et al.,
65 1999) because the presence of emergent vegetation (such as trees), to a certain extent, narrows
66 the channel width, thereby altering flow properties.

67 This study aims to develop a depth-averaged 2D numerical model for river hydraulics and
68 morphology with vegetation effects, and to better understand the effects of vegetation on
69 changing river morphology through intensive numerical experiments. The numerical model is
70 built upon a layer-based 2D hydro-morphodynamic model (LHMM) (Guan et al., 2014; Guan et
71 al., 2015b) which has been validated by a variety of flood events. A vegetation module is
72 developed and incorporated in the model system to simulate vegetation effects. The model is
73 validated against several laboratory experiments before a real-world application is considered.

74

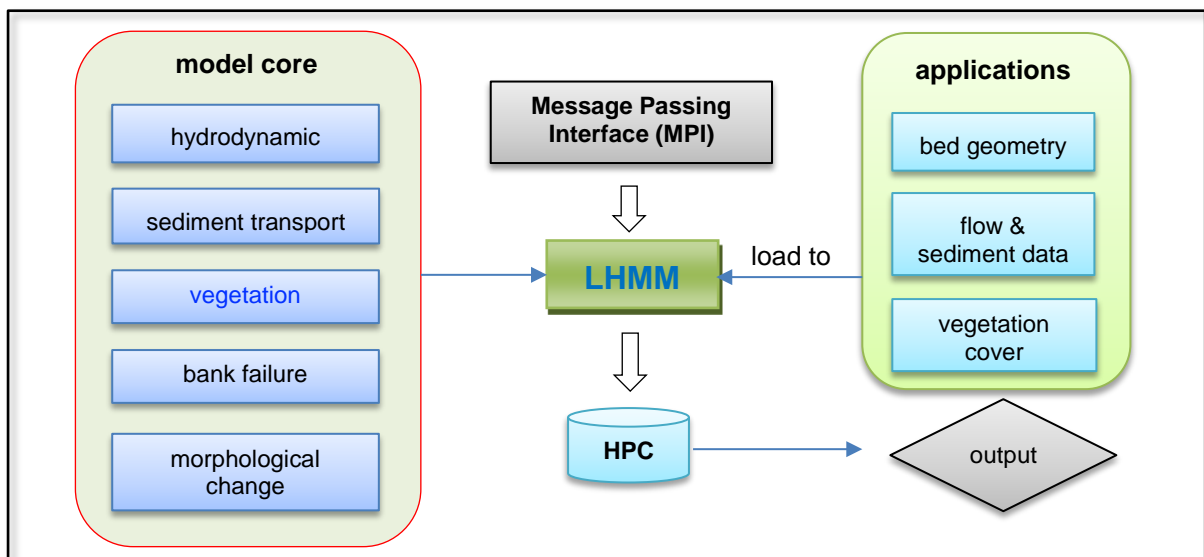
75 **2. Numerical Model (LHMM)**

76 **2.1. Model framework**

77 Shallow water based numerical models have been widely used for river flow modelling (Costabile
78 and Macchione, 2015; Guan et al., 2013; Hou et al., 2015; Vacondio et al., 2014). The layer-based
79 hydro-morphodynamic model (LHMM) that has been presented in previous work (Guan et al.,
80 2014, 2015a; Guan et al., 2015b) also solves the fully coupled shallow water equations (SWEs)
81 and the sediment transport formulation. Herein, a new vegetation model component is developed

82 and included in LHMM to consider the vegetation effects. The model system considers the mass
 83 and momentum exchange of non-cohesive sediment between bed and flow, and updates the
 84 hydraulic and sediment quantities per grid cell, per time step. Figure 1 shows the entire LHMM
 85 model framework, which includes four modules:

- 86 • **Hydrodynamic module:** The depth-averaged 2D shallow water equations are solved to
 87 predict rapidly varying unsteady flows, taking into account the feedback from sediment
 88 and vegetation.
- 89 • **Sediment transport module:** A non-uniform sediment transport model is developed to
 90 describe the transport of sediment particles.
- 91 • **Vegetation module:** The external force exerted by vegetation on flow and sediment is
 92 parameterised.
- 93 • **Bank failure module:** Is a model component to simulate lateral bank erosion or failure.
- 94 • **Bed deformation module:** The bed elevation is updated after localised erosion and
 95 deposition of sediment.



96

97

Figure 1. Model framework of LHMM

98 2.2. Hydrodynamic module

99 The hydrodynamic module solves the depth-averaged 2D shallow water equations, including the

100 effects of sediment and vegetation on flow dynamics. In a vector form, the governing equations
 101 can be expressed by

$$\frac{\partial \mathbf{U}}{\partial t} + \frac{\partial \mathbf{E}}{\partial x} + \frac{\partial \mathbf{F}}{\partial y} = \frac{\partial \tilde{\mathbf{E}}}{\partial x} + \frac{\partial \tilde{\mathbf{F}}}{\partial y} + \mathbf{S}_o + \mathbf{S}_f + \mathbf{S}_v + \mathbf{S}_{fb} \quad (1)$$

102 where

$$\mathbf{U} = \begin{bmatrix} \eta \\ hu \\ hv \end{bmatrix}, \mathbf{E} = \begin{bmatrix} hu \\ hu^2 + \frac{1}{2}gh^2 \\ huv \end{bmatrix}, \mathbf{F} = \begin{bmatrix} hv \\ huv \\ hv^2 + \frac{1}{2}gh^2 \end{bmatrix}, \tilde{\mathbf{E}} = \begin{bmatrix} 0 \\ h(T_{xx} + D_{xx}) \\ h(T_{xy} + D_{xy}) \end{bmatrix}, \tilde{\mathbf{F}} = \begin{bmatrix} 0 \\ h(T_{yx} + D_{yx}) \\ h(T_{yy} + D_{yy}) \end{bmatrix}$$

$$\mathbf{S}_o = \begin{pmatrix} 0 \\ -gh \frac{\partial z_b}{\partial x} \\ -gh \frac{\partial z_b}{\partial y} \end{pmatrix}, \mathbf{S}_f = \begin{pmatrix} 0 \\ -ghS_{fx} \\ -ghS_{fy} \end{pmatrix}, \mathbf{S}_v = \begin{pmatrix} 0 \\ -\frac{\tau_{vx}}{\rho_w} \\ -\frac{\tau_{vy}}{\rho_w} \end{pmatrix}$$

$$\mathbf{S}_{fb} = \begin{pmatrix} 0 \\ \frac{\Delta \rho u}{\rho} \frac{\partial z_b}{\partial t} [\alpha(1-p) - c] - \frac{\Delta \rho gh^2}{2\rho} \frac{\partial c}{\partial x} - S_a \\ \frac{\Delta \rho v}{\rho} \frac{\partial z_b}{\partial t} [\alpha(1-p) - c] - \frac{\Delta \rho gh^2}{2\rho} \frac{\partial c}{\partial y} - S_b \end{pmatrix} \quad (2)$$

105 where \mathbf{U} is the vector of conserved variables; \mathbf{E} and \mathbf{F} are the flux vectors of the flow in the x and
 106 y directions respectively, $\tilde{\mathbf{E}}$ and $\tilde{\mathbf{F}}$ contain the turbulent and dispersion terms in the x and y
 107 directions, \mathbf{S}_o and \mathbf{S}_f are the vectors containing the bed slope terms and the frictional slope
 108 terms, \mathbf{S}_v contains vegetation terms, and \mathbf{S}_{fb} is the vector of flow-bed interaction terms. In these
 109 vector terms, h = flow depth, z_b = bed elevation, η = water surface elevation, u and v = the depth-
 110 averaged flow velocity components in the two Cartesian directions, T_{xx} , T_{xy} , T_{yx} and T_{yy} are the
 111 depth-averaged turbulent stresses, D_{xx} , D_{xy} , D_{yx} and D_{yy} are the dispersion terms due to the
 112 effect of secondary flow, ρ = sediment porosity, c = total volumetric sediment concentration, τ_{vx}
 113 and τ_{vy} are the vegetation shear stresses in the x and y directions; ρ_s and ρ_w denote the
 114 densities of sediment and water respectively, $\Delta \rho = \rho_s - \rho_w$, ρ = density of flow-sediment mixture, α
 115 = sediment-to-flow velocity ratio determined by

$$\alpha = \frac{u^*}{u} \frac{1.1(\theta/\theta_{cr})^{1.7} [1 - \exp(-5\theta/\theta_{cr})]}{\sqrt{\theta_{cr}}} \quad (3)$$

117 where θ and θ_{cr} represent the real dimensionless bed shear stress, and the critical Shields
 118 parameter, u^* is shear velocity. S_a and S_b are the additional terms related to the velocity ratio
 119 defined by Guan et al. (2014)

$$\begin{aligned}
120 \quad S_a &= \frac{\Delta \rho u}{\rho} (1 - \alpha) [c \nabla \cdot (h \mathbf{V}) - (h \mathbf{V}) \nabla \cdot \mathbf{C}] \\
121 \quad S_b &= \frac{\Delta \rho v}{\rho} (1 - \alpha) [c \nabla \cdot (h \mathbf{V}) - (h \mathbf{V}) \nabla \cdot \mathbf{C}] \quad (4)
\end{aligned}$$

122 where $\nabla = \vec{i}(\partial/\partial x) + \vec{j}(\partial/\partial y)$; \mathbf{C} is the sediment concentration vector defined by $\mathbf{C} = c(\vec{i} + \vec{j})$; \mathbf{V} is
123 the velocity vector defined by $\mathbf{V} = u\vec{i} + v\vec{j}$.

124 The depth-averaged turbulent stresses are determined by the Boussinesq approximation which
125 has been widely used in the literature (e.g. (Abad et al., 2008; Begnudelli et al., 2010; Wu,
126 2004)). This gives the Reynolds stresses as:

$$T_{xx} = -2(v_t + \nu) \frac{\partial u}{\partial x} \quad (5a)$$

$$T_{xy} = T_{yx} = -(v_t + \nu) \left(\frac{\partial u}{\partial x} + \frac{\partial v}{\partial x} \right) \quad (5b)$$

$$T_{yy} = -2(v_t + \nu) \frac{\partial v}{\partial x} \quad (5c)$$

127 where v_t is the turbulence eddy viscosity and ν is the molecular viscosity, which can be ignored in
128 environmental applications. Various approaches have been adopted to estimate the turbulence
129 viscosity, e.g. assuming a constant eddy viscosity, an algebraic turbulence model ($v_t \sim hu^*$), as
130 well as the $k - \varepsilon$ turbulence model. In this study, the eddy viscosity is estimated by $v_t = \beta hu^*$ with
131 $\beta = 0.5$. The dispersion terms are generally delivered from the difference of the depth-averaged
132 velocity and the vertical varying velocity as follows:

$$D_{xx} = \frac{1}{h} \int_{z_0}^{z_0+h} [u(z) - u]^2 dz \quad (6a)$$

$$D_{xy} = D_{yx} = \frac{1}{h} \int_{z_0}^{z_0+h} [u(z) - u] [v(z) - v] dz \quad (6b)$$

$$D_{yy} = \frac{1}{h} \int_{z_0}^{z_0+h} [v(z) - v]^2 dz \quad (6c)$$

133 where z_0 is the zero velocity level; $u(z)$ and $v(z)$ represents the x and y components of the
134 vertically varying velocity respectively. A number of approaches have been proposed to calculate
135 the vertical varying velocity both in the streamwise and transverse directions (e.g. (De Vriend,
136 1977; Guymer, 1998; Odgaard, 1986; Wu et al., 2005a)). The Odgaard's equation, based on the

137 linear transverse velocity profiles over the depth, is employed in this work because of its
 138 robustness and simplicity. The longitudinal and transverse velocities are given as (Odgaard,
 139 1986):

$$u_l(z) = U \frac{m+1}{m} \xi^{1/m} \quad (7a)$$

$$u_t(z) = 2v_s \left(\xi - \frac{1}{2} \right), \quad v_s = U \frac{2m+1}{2\kappa^2 m} \frac{h}{r_c} \quad (7b)$$

140 where $u_l(z)$ and $u_t(z)$ are the longitudinal and transverse velocity components in the streamline
 141 coordinates, respectively; U is the depth-averaged longitudinal velocity; $m = \kappa C/g^{0.5}$ with $\kappa = 0.41$
 142 being the von Karman's constant; v_s represents the transverse velocity at the free surface; $\xi = (z -$
 143 $z_0)/h$ is the dimensionless distance from the bed; r_c is the radius of curvature. Following the study
 144 (Begnudelli et al., 2010), integration of Eqs. (6) using the velocity profiles Eq. (7) yields:

$$D_{ll} = \frac{U^2}{m(2+m)}; \quad D_{lt} = D_{tl} = \frac{Uv_s}{1+2m}; \quad D_{tt} = \frac{v_s^2}{3} \quad (8)$$

145 Defining the angle of the depth-averaged velocity vector measured counter-clockwise from the x
 146 direction as φ , the dispersion terms in the curvilinear coordinates can then be converted to the
 147 Cartesian coordinate system by:

$$\begin{bmatrix} D_{xx} & D_{xy} \\ D_{yx} & D_{yy} \end{bmatrix} = \mathbf{M}(\varphi) \begin{bmatrix} D_{ll} & D_{lt} \\ D_{tl} & D_{tt} \end{bmatrix} \mathbf{M}^T(\varphi)$$

148 where $\mathbf{M}(\varphi) = \begin{bmatrix} \cos \varphi & -\sin \varphi \\ \sin \varphi & \cos \varphi \end{bmatrix}$, so this leads to:

$$D_{xx} = D_{ll} \cos^2 \varphi - 2D_{lt} \sin \varphi \cos \varphi + D_{tt} \sin^2 \varphi \quad (9a)$$

$$D_{xy} = (D_{ll} - D_{tt}) \sin \varphi \cos \varphi + D_{lt} (\cos^2 \varphi - \sin^2 \varphi) \quad (9b)$$

$$D_{yy} = D_{ll} \sin^2 \varphi + 2D_{lt} \sin \varphi \cos \varphi + D_{tt} \cos^2 \varphi \quad (9c)$$

149 Eqs.(9) accounts for the effect of secondary flow which is included in the hydrodynamic
 150 governing equations.

151 2.3. Sediment transport module

152 The governing equation of the i th size sediment class is written according to the velocity ratio α

153 by

$$\frac{\partial hc_i}{\partial t} + \frac{\alpha \partial huc_i}{\partial x} + \frac{\alpha \partial hvc_i}{\partial y} = - \frac{\alpha(q_{bi} - F_i q_{b*i})}{L_i} \quad (10)$$

154 where c_i = depth-averaged volumetric bedload concentration of the i^{th} size class; $q_{bi} = h\bar{U}c_i$ =
 155 real sediment transport rate of the i^{th} fraction; $\bar{U} = \sqrt{u^2 + v^2}$ is the depth-averaged velocity; q_{b*i} =
 156 sediment transport capacity of the i^{th} fraction; F_i represents the proportion of i^{th} grain-size fraction
 157 in the total moving sediment and is updated at each time step using the approach presented by
 158 Wu (2004); L_i = non-equilibrium adaptation length of sediment transport of the i^{th} fraction which is
 159 estimated by

$$L_i = \frac{h\sqrt{u^2 + v^2}}{\gamma\omega_{f,i}} \text{ with } \gamma = \min\left(\alpha \frac{h}{h_b}, \frac{1-p}{c}\right) \quad (11)$$

160 where h_b is the thickness of a sheet flow layer; ω_{fi} is the effective settling velocity of a sediment
 161 particle which is determined by the formula proposed by Soulsby (1997):

$$\omega_{fi} = \frac{v}{d_i} \left(\sqrt{10.36^2 + 1.049(1-c)^{4.7}d_*^3} - 10.36 \right) \quad (12)$$

162 where $d_* = d_i[(s-1)g/v^2]^{1/3}$ is the dimensionless particle diameter.

163 The bed load is estimated using the Meyer-Peter & Müller equation (Meyer-Peter and Müller,
 164 1948)

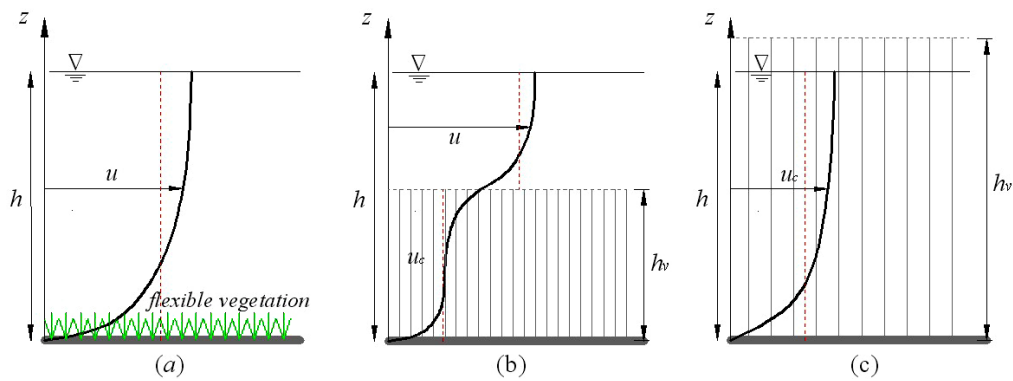
$$q_{b*i} = 8(\theta_i - \theta_{cr,i})^{1.5} \sqrt{(s-1)gd_i^3} \quad (13)$$

165 where $\theta_{cr,i}$ is the critical dimensionless bed shear stress of the i^{th} fraction; θ is the dimensionless
 166 bed shear stress; $s = (\rho_s/\rho_w - 1)$ is the special gravity of sediment.

167 2.4. Vegetation module

168 In the current model framework, vegetation is catalogued into two types according to the stiffness
 169 and submerged extent: (i) submerged flexible vegetation, such as grass; (ii) submerged or
 170 emergent plants with rigid or hard stems (rigid vegetation). The vertical distribution of flow
 171 velocity in the two types of vegetation is sketched in Figure 2. In case of submerged flexible

172 vegetation, the existence of vegetation elevates the total resistance, thereby reducing the flow
 173 velocity. For the flow over submerged rigid plants, the velocity in the lower layer of the plants is
 174 obviously decreased because of the resulting drag force and the effect caused by narrowed
 175 channel width. The decreased velocity can reduce bed shear stress, and subsequently weaken
 176 the sediment transport capability of the flow. In the case of emergent rigid plants, the main
 177 feature of velocity distribution is similar to that in Figure 2(a), but the magnitude of velocity may
 178 be significantly affected by plants and hence different, as shown in Figure 2(c). When
 179 considering vegetation in flow modelling, a common approach is to treat vegetation as rigid
 180 cylinders with the same diameter, same species and same spacing (Bennett et al., 2008; Choi
 181 and Kang, 2006; Wu et al., 2005b).



182

183 Figure 2 Flow velocity distribution with vegetation: (a) flow over submerged flexible vegetation; (b)
 184 flow over submerged rigid plants; (c) flow through emergent rigid plants

185 **2.4.1. Bed shear stress effective to sediment transport**

186 In Eq. (2), the shear stresses related to grain roughness and vegetation roughness are treated
 187 separately. In other words, the flow resistance is divided to two parts to obtain the appropriate
 188 Manning's n , i.e. the resistance exerted by the bed and the resistance exerted by the vegetation.
 189 This method has been adopted by many other studies (Crosato and Saleh, 2011; Li and Millar,
 190 2011) because it can not only reflect the decreasing of bed shear stress which reduces the
 191 sediment transport capacity in the vegetation layer, but also elucidate the increasing of total
 192 resistance which reduces flow velocity within and above plants. The final expression of the
 193 Manning coefficient is given by

$$n = \sqrt{n_1^2 + n_2^2} \quad (14)$$

194 where n_1 is the Manning's coefficient related to grain roughness; n_2 is the Manning's coefficient
 195 associated with the flexible vegetation roughness. Whilst for the rigid plants, the vegetation shear
 196 stress τ_b is calculated by formula below

$$\tau_b = \frac{\rho_w g n_1^2 \mathbf{U}_c |\mathbf{U}_c|}{h^{1/3}} \quad (15)$$

197 The corresponding dimensionless bed shear stress is calculated by

$$\theta_i = \frac{|\tau_b|}{\rho_w g (s-1) d_i} = \frac{n_1^2 |\mathbf{U}_c|^2}{(s-1) d_i h^{1/3}} \quad (16)$$

198 where \mathbf{U}_c is the vector of depth-averaged flow velocity in the vegetation layer; for emergent
 199 vegetation, it is equal to the depth-averaged flow velocity \mathbf{U} ; $|\mathbf{U}_c|$ is the magnitude of \mathbf{U}_c
 200 determined using the Stone and Shen's equation (Stone and Shen, 2002).

$$\mathbf{U}_c = \delta \mathbf{U} \sqrt{\left(\frac{h_v}{h}\right)} \quad (17)$$

201 in which, δ is a coefficient approximately equal to 1.0; h_v represents the height of rigid plants.
 202 When calculating the sediment transport rate, the velocity in the vegetation layer will be used
 203 instead of the depth-averaged flow velocity.

204 **2.4.2. Parameterisation of vegetation shear stress**

205 In the current model system, the vegetation is parameterised according to the classification of
 206 vegetation. The effects of flexible vegetation are represented through the shear stress related to
 207 the vegetation roughness by

$$\tau_v = \frac{\rho_w g n_2^2 \mathbf{U} |\mathbf{U}|}{h^{1/3}} \quad (18)$$

208 For rigid plants, individual elements of plants are identified as disperse obstacles with drag
 209 forces, but this will be spatially averaged to give a shear stress per unit volume of water as

$$\tau_v = \frac{1}{2} \rho_w \lambda C_D h |\mathbf{U}_c| \mathbf{U}_c \quad (19)$$

210 where C_D represents the drag coefficient of vegetation elements; λ denotes the projected area of
 211 vegetation elements per unit volume of water, given by

$$\lambda = \frac{4\alpha_v V_d}{\pi D_v} \quad (20)$$

212 where α_v is a shape factor, V_d represents the vegetation density in vegetated zones (%), D_v is the
 213 diameter of the plant stems; l and w are the length and width of vegetated channel, respectively.
 214 Therefore, the vegetation shear stress τ_{vx} and τ_{vy} exerted by rigid plants in Eq. (1) are calculated
 215 by

$$\tau_{vx} = \frac{1}{2} \rho_w \lambda C_D h u_c \sqrt{u_c^2 + v_c^2} \quad (21a)$$

$$\tau_{vy} = \frac{1}{2} \rho_w \lambda C_D h v_c \sqrt{u_c^2 + v_c^2} \quad (21b)$$

216 where u_c and v_c are the depth-averaged flow velocity in the vegetation layer in the x and y
 217 directions. Previous studies (Alonso, 2004; Garcia et al., 2004; Lopez and Garcia, 2001) have
 218 demonstrated that the drag coefficient C_D is usually in the range of 0.8 and 3.5, and typically
 219 varies from 1 to 1.5 (Garcia et al., 2004).

220 2.5. Bed deformation module

221 The erosion and deposition process is calculated per grid cell at each time step to update the
 222 new bed elevation based on the results from the previous hydrodynamic model, sediment
 223 transport model and vegetation model. The bed deformation is calculated by

$$\frac{\partial z_b}{\partial t} = \frac{1}{1-p} \sum_{i=1}^N \left[\frac{(q_{bi} - F_i q_{b*i})}{L_i} \right] \quad (22)$$

224 where the values of the parameters in the right hand side are calculated according to the
 225 equations already explained in previous sections.

226 2.6. Lateral bank erosion

227 Bank erosion is one of the key morphological processes affecting the evolution of river channels,
 228 particularly river banks. In reality, bank failure is a complex process which is closely related to
 229 many physical factors, such as vegetation and soil properties. Since this study aims to

230 investigate the physical process of flow and sediment transport in the presence of vegetation, we
231 adopt a simplified bank failure model to represent the lateral bank erosion. The principle of the
232 adopted method is that if the bank slope becomes steeper than the critical angle of failure, the
233 bank will fail to form a new bedform with a slope approximately equal to the critical angle of
234 repose. The bank failure process is simulated according to this principle, while maintaining mass
235 conservation of sediment material. Different values are used for 1) the critical angles that initiate
236 bank failure, and 2) the reformation bed angles above and below the water. Here, the wet and
237 dry conditions are defined according to the simulated water depth at each time step. The bank
238 failure model is described in detail in Guan et al. (2014).

239 **2.7. Model solution procedure**

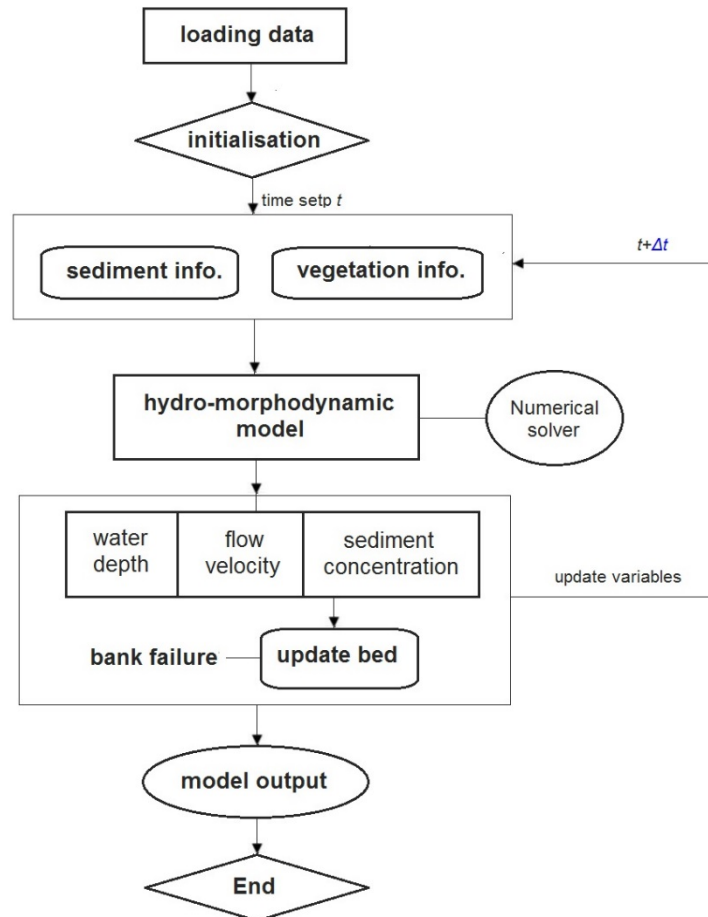
240 The model's governing equations (Eqs.1,10, 22) are solved numerically by a well-balanced
241 Godunov-type finite volume method (FVM) on Cartesian grids and details can be found in
242 previous publications (Guan et al., 2013, 2014). As shown in Figure 3, the computation
243 procedure at each time step consists of the following steps:

- 244 (1) Load the data files (hydraulics, sediment, vegetation cover) to the model;
- 245 (2) Calculate shear stresses exerted by the bed (Eq.15) and the vegetation (Eq.18, 19);
- 246 (3) Calculate sediment transport rate and capacity in each cell;
- 247 (4) Solve the coupled governing equations (Eqs.1,10) to update hydraulic variables and
248 sediment concentration to the new time step;
- 249 (5) Update the bed elevation using Eq.(22);
- 250 (6) Activate the bank failure module if bank erosion occurs;
- 251 (7) Update the changes in river morphology;
- 252 (8) Return to step (1) and start the calculation at a new time step
- 253 (9) Repeat step (1) to (8) until the end of the simulation.

254 As the numerical scheme is explicit, the numerical stability of the model system is controlled by
255 the CFL condition, which may be used to determine the time step Δt at each time step using the
256 following equation

$$\Delta t = CFL \min \left(\min \frac{dx_i}{|u_i| + \sqrt{gh_i}}, \min \frac{dy_j}{|v_j| + \sqrt{gh_j}} \right) \quad (25)$$

257 The Courant number $0 < CFL < 1.0$ is implemented for flow calculation, taking into account
 258 additional conditions for sediment transport and bed change.



259

260

Figure 3 Workflow diagram of LHMM model core

261 3. Results and Discussion

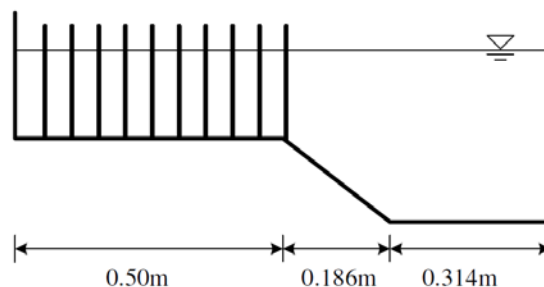
262 3.1. Model validation

263 In this section, the new hydraulics-morphology-vegetation modelling system is validated against
 264 a number of laboratory-scale test cases, including steady flow over a compound channel with a
 265 fixed bed (Pasche and Rouvé, 1985) and steady flow over a compound channel with a movable
 266 bed (Bennett et al., 2008).

267 **3.1.1. Flow over a compound channel with a vegetated floodplain**

268 The experiments conducted by Pasche and Rouvé (1985) are first considered to verify the
 269 capability of the model in accurately simulating shallow flow hydrodynamics in the presence of
 270 vegetation. The experiment was carried out in a 25.5 m x 1.0 m compound channel with a
 271 floodplain covered by vegetation. The cross-section of the channel is shown in Figure 4. Circular
 272 wooden cylinders with a uniform diameter of 0.012 m are used to represent the vegetation in the
 273 floodplain. Two experimental cases are considered in this work: Case 1 has a vegetative density
 274 of 0.0126 and bed slope of 0.001; Case 2 has a vegetative density of 0.0253, and bed slope of
 275 0.0005. For both cases, the initial water depth is 0.2 m in the main channel and 0.076 m in the
 276 floodplain and an inflow discharge of 0.0345 m³/s is fed from the upstream boundary to drive the
 277 steady flow.

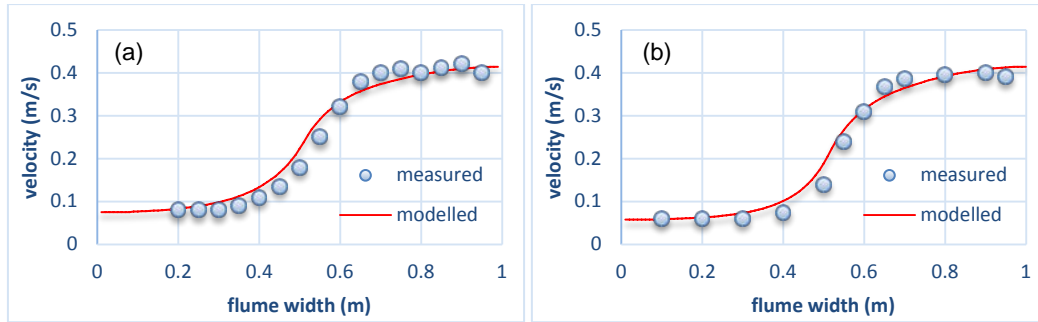
278 During the simulations, the key coefficients for the channel and floodplain are specified as
 279 follows: for the simple cylindrical vegetation, shape factor = 1.0; Manning's $n = 0.01$; drag
 280 coefficient $C_d = 1.5$. The experimental flume is discretised using a mesh with 255 x 100 uniform
 281 cells of 0.1 m x 0.01 m. Figure 5 presents the simulations results for both of the experiments,
 282 where the modelled cross-section velocity profiles are compared satisfactorily with the laboratory
 283 measurements. The velocity in the vegetated zone is significantly smaller than that in the main
 284 channel, and the flow velocity in the vegetated floodplain decreases with higher vegetated
 285 density (Figure 5(b)). Successful simulation of this laboratory test demonstrates that the
 286 proposed model is capable of accurately simulating shallow flow hydrodynamics in the presence
 287 of vegetation.



288

289

Figure 4. Cross-section of the flume used in the experiment of Pasche and Rouve (1995).



290

291 Figure 5. Measured and modelled velocity profiles for the two experiments with different vegetation density: (a)

292

Case 1 (vegetative density of 0.0126); (b) Case 2 (vegetative density of 0.0253).

293

3.1.2. Fluvial response to in-stream woody vegetation

294

A series of experiments have been conducted in the hydraulic laboratory of Buffalo University to

295

examine in detail the response of a stream corridor to woody vegetation of various configurations

296

(e.g. (Bennett et al., 2002; Bennett et al., 2008)). These experiments provide further valuable

297

datasets for the validation of the current hydraulics-morphology-vegetation modelling system.

298

The experiments reported in Bennett et al. (2008) are considered herein to verify model

299

capability in predicting alluvial response to riparian vegetation.

300

The experiments were performed in a flume which is 10 m long, 0.63 m wide and 0.61 m deep.

301

The channel was first filled with a 0.5 m thick pre-wetting layer of sands with a uniform grain

302

diameter of 0.8 mm. A 5 m long trapezoidal channel was cut out from the sand layer using an

303

aluminium plate mounted on a movable carriage above the flume. The trapezoidal sand channel

304

had a top width of 0.312 m, a bottom width of 0.1 m and a side slope of 3:1.

305

An adjustable weir was installed to control the flow depth, which was initially 0.069 m in the main channel, A

306

constant inflow ($Q = 0.0033 \text{ m}^3/\text{s}$) was imposed from the upstream boundary of the channel. In

307

the experiments, the channel was covered by three vegetation zones where emergent, rigid

308

wooden dowels with a diameter of 5 mm were planted. Two zones were on the left and one on

309

the right, with each spaced 1.5 m apart. Vegetation zones of different shapes were used in the

310

experiments, two of which are modelled in this work: (1) 0.5 m \times 0.25 m rectangle; (2) 0.5 m

311

diameter semicircle. For both cases, the vegetation density is chosen to be 0.0294.

312

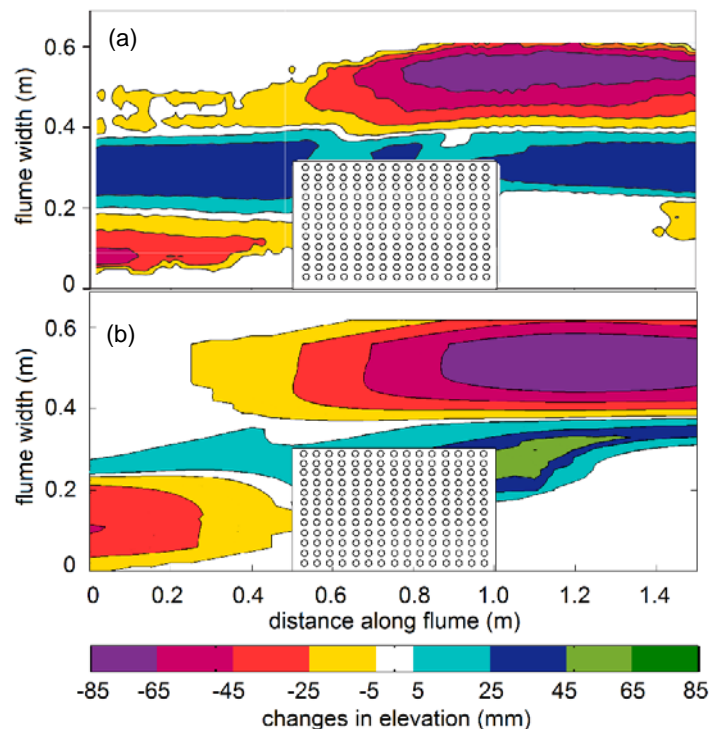
Both simulations last for 6600s, the flume is discretised by a mesh of 0.05 m \times 0.01 m uniform

313

cells. The experiment indicates that no sediment transport occurs in the absence of vegetation.

314 To ensure this, the manning's n is set to 0.028. The shape factor and drag coefficient are
 315 respectively set to 1.2 and 2.0.

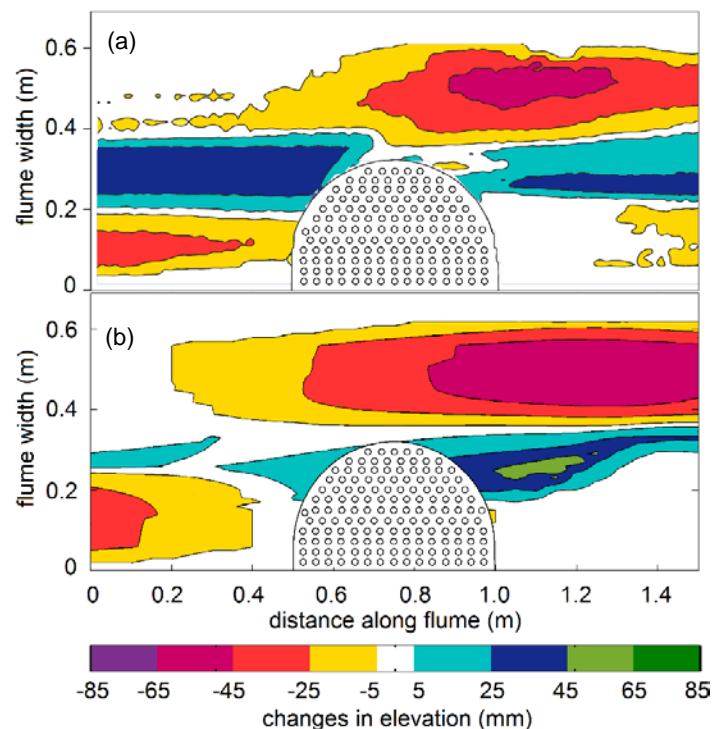
316 Figure 6 demonstrates the modelled and measured changes in channel bed elevation in the
 317 presence of the rectangular vegetation zone. It is clearly shown that the modelled bed changes
 318 are generally in good agreement with observations, in terms of both the pattern and magnitude of
 319 net erosion and deposition. Around the rectangular vegetation zone, the model predicts two
 320 erosion patches that closely agreed with the measurements, one in the opposite side of the
 321 vegetation zone and another in the upstream bank area. However, although the deposition in the
 322 mid-channel region is correctly modelled, the deposition depth upstream of the vegetation zone
 323 is predicted to be smaller than the observed results; additionally the model slightly overestimates
 324 the mid-channel deposition downstream of the vegetation zone. As a whole, the current model
 325 simulates reasonably well the alluvial process in response to riparian vegetation in this case,
 326 considering the various uncertainties existing in sediment transport models.



327
 328 Figure 6. Contour plots of changes in channel bed elevation in the presence of rectangular vegetation: (a)
 329 observed result; (b) simulation result.

330 With identical model parameters, the model simulates the case presented with a semicircle
 331 vegetation zone. The predicted bed changes are shown in Figure 7, in comparison with the

332 laboratory measurement. The current model again predicts the general pattern of the channel
 333 erosion and deposition around the vegetation zone reasonably well. As with the rectangular
 334 vegetation patch case, discrepancies between the modelled and measured results are observed
 335 in the mid-channel deposition zone. Further comparison is made in Figure 8 by plotting the
 336 measured and predicted bed profiles at three cross-sections which are located at the front (- 0.5
 337 m) (CS1), the middle (0 m) (CS2) and the back (0.5 m) (CS3) of the semicircle vegetation zone.
 338 Clearly, the predicted bed profiles agree with the measurements reasonably well. Particularly,
 339 erosion takes place at the left bank while deposition is found in the mid-channel at CS1; at both
 340 CS2 and CS3, erosion happens at the right bank which is accurately predicted, but the model
 341 slightly overestimates the deposition at CS2. Overall, successful reproduction of these two tests
 342 confirms that the present model is capable of simulating morphological changes in the presence
 343 of vegetation. From the results, it may be concluded that riparian vegetation has a significant
 344 effect on the morphological change of the river corridor.



345
 346 Figure 7. Contour plots of changes in channel bed elevation in the presence of semicircle vegetation: (a)
 347 observed result; (b) modelled result.

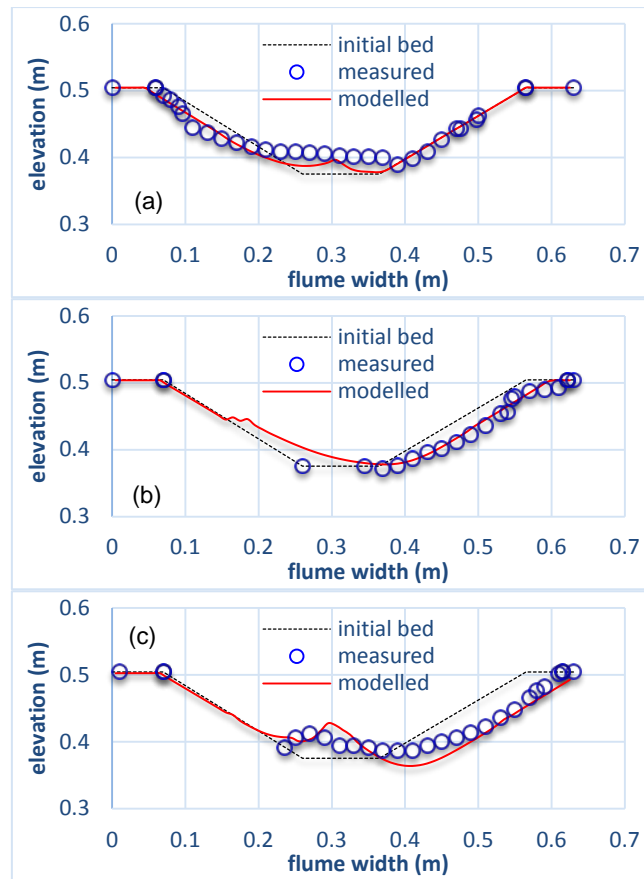


Figure 8. Modelled and measured bed profiles at (a) the front (-0.5 m), (b) the middle (0 m) and (c) the back (+0.5 m) of the vegetation zone

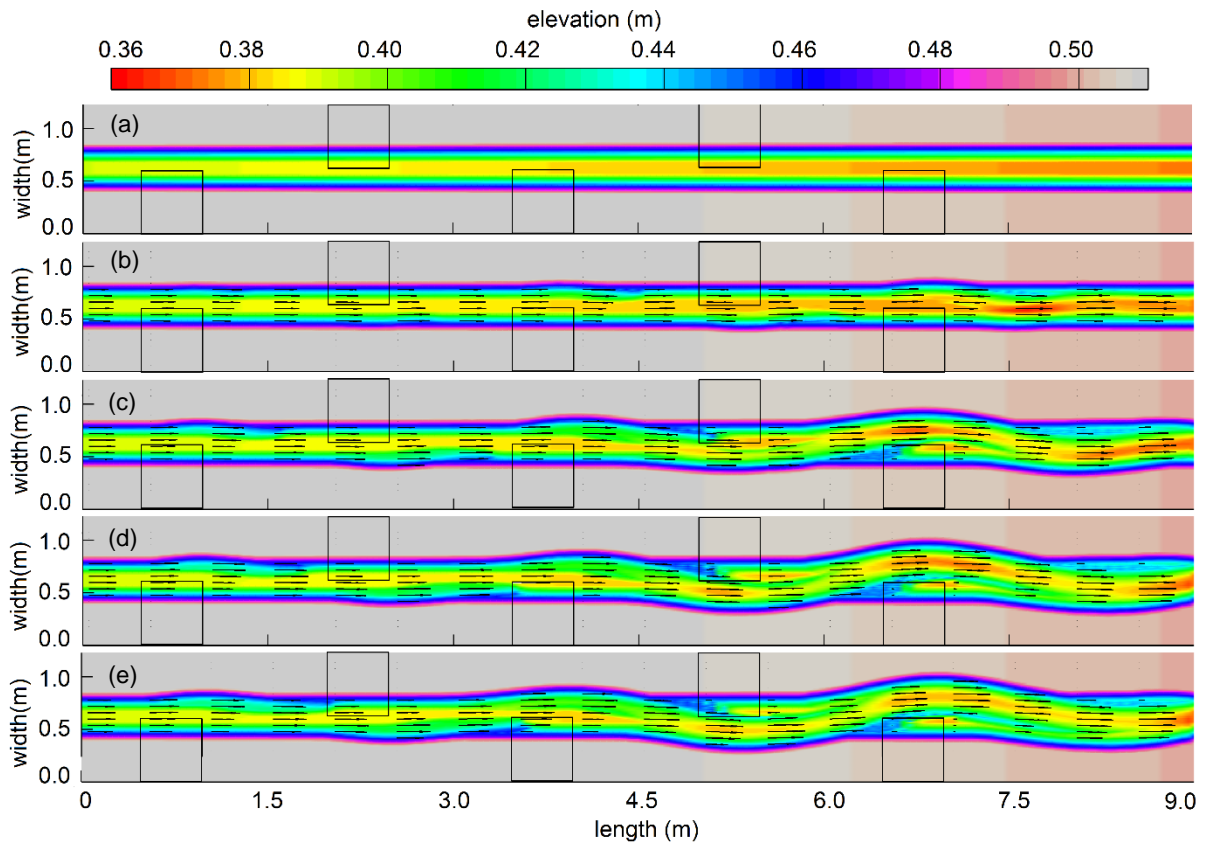
3.2. Channel pattern adjustment to riparian vegetation

Based on the validation cases presented above, numerical experiments with different vegetation covers are designed to further explore the effects of riparian vegetation on channel pattern adjustment at a wider context. The simulations are parameterised with the same main channel shape, the same streamwise bed slope, and the same sediment material as the experimental cases considered in 3.1.2. But the length of the erodible bed is extended from 5 m to 9 m, and the floodplain width from 0.07 m to 0.37 m at both sides in order to investigate the lateral bank erosion. Five vegetation zones are placed at both sides of the main channel. The location of these five vegetation zones and the initial channel are illustrated in Figure 9(a). Each vegetation patch has the same vegetation density, plant diameter and drag coefficient.

Figure 9 presents the snapshots of the simulation results at different output times, demonstrating changes in channel pattern in response to the five emergent, woody vegetation zones. Overall,

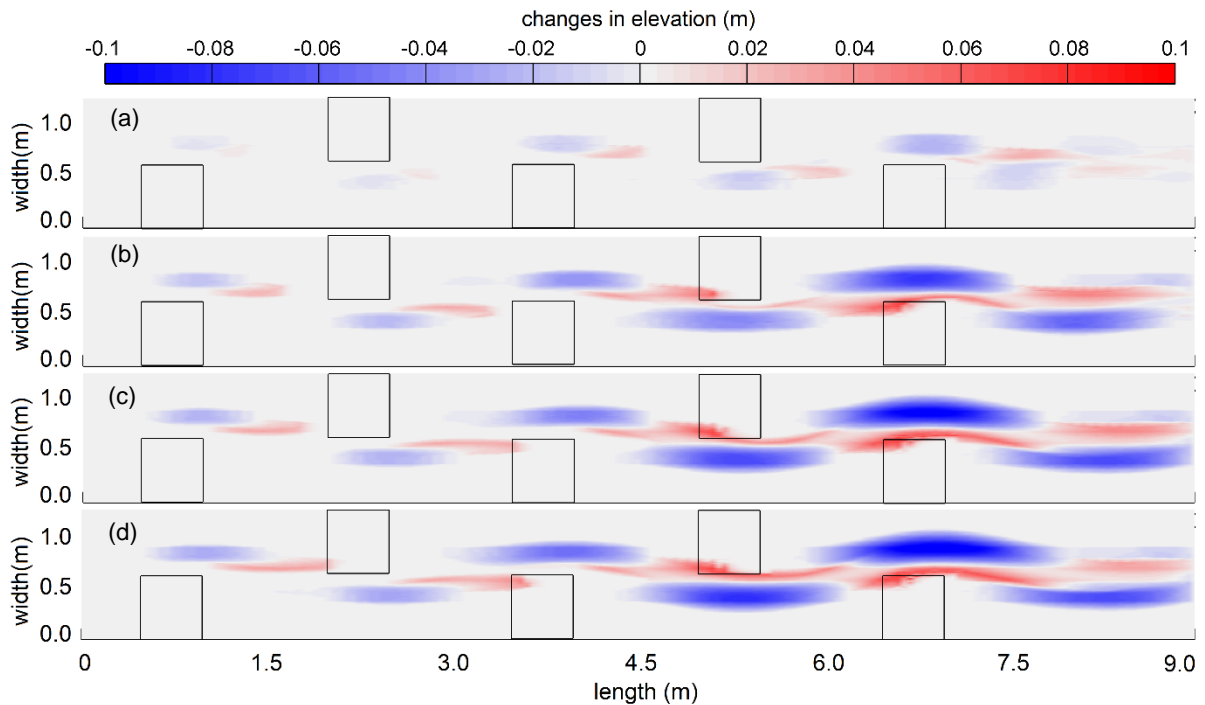
365 the presence of vegetation patches forces the channel to become meandering after initially being
366 straight. The presence of vegetation changes the flow field by increasing velocity at the opposite
367 size of the vegetation zones, but reducing the velocity within the vegetation zones. Accordingly,
368 the modified flow field leads to the deformation of the channel corridor. Figure 10 further shows
369 the erosion and deposition patterns in the channel at different output times. It is clear that the
370 eroding process dominates channel changes at the opposite sides of the vegetation zones and
371 that erosion becomes more severe and tends to be in a steady state over the time. Meanwhile,
372 deposition occurs around the vegetation, which can be attributed to two main causes: (1) the
373 deposition in front of the vegetation zone is caused by blockage effects of the vegetation; (2)
374 since the initial bank slope is approximately equal to the angle of repose of the sediment, bed
375 erosion initiates the repose and retreatment of the lateral bank which subsequently leads to
376 some deposition at the bank toe.

377 From the numerical experiments, the downstream channel is observed to be more intensively
378 meandering. This is because the change in velocity at the downstream is more significant due to
379 the presence of vegetation upstream. This indicates that vegetation can pose consistent and
380 cumulative effects on the morphological changes to a river corridor. From the simulation results,
381 it is clearly seen that the thalweg of the stream corridor is gradually changed from a straight line
382 to a meandering curve with a wavelength equal to the interval of vegetation zones. Furthermore
383 the channel is significantly widened, particularly at the downstream, which is consistent with the
384 forms of natural river systems.



385

386 Figure 9. Channel pattern adjustment in response to multiple vegetation patches along a straight river corridor.

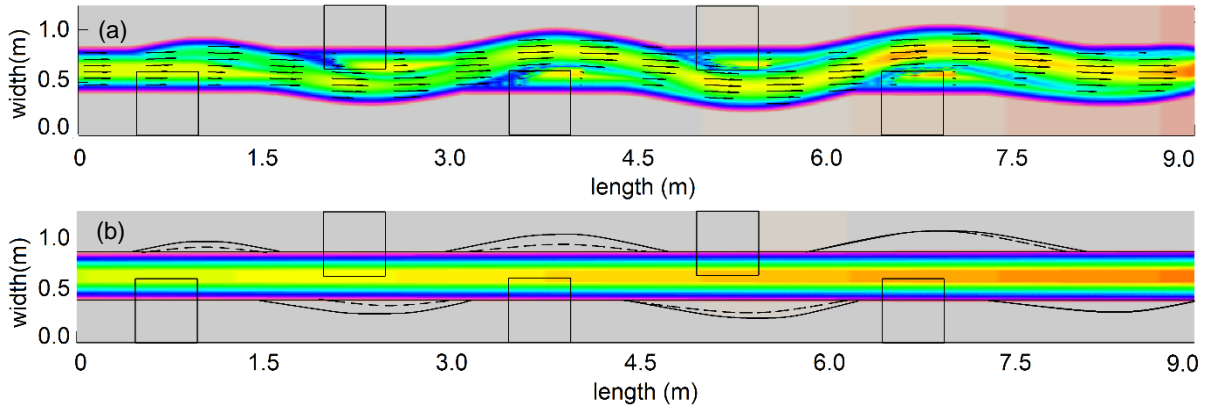


387

388 Figure 10. Erosion and deposition of the channel in response to the vegetation against time.

389 The alluvial response to the vegetation zone is more remarkable under the condition of higher
 390 inflow discharge, as demonstrated in Figure 11. Compared with the lower inflow (Q_{in}), the higher

391 inflow discharge ($1.5Q_{in}$) induces more severe lateral bank erosion, particularly near the
 392 upstream vegetation zones. Both bank erosion width and size are much larger near the first four
 393 vegetation zones for the $1.5Q_{in}$ inflow. However, the difference becomes smaller after the fifth
 394 vegetation patch.



395

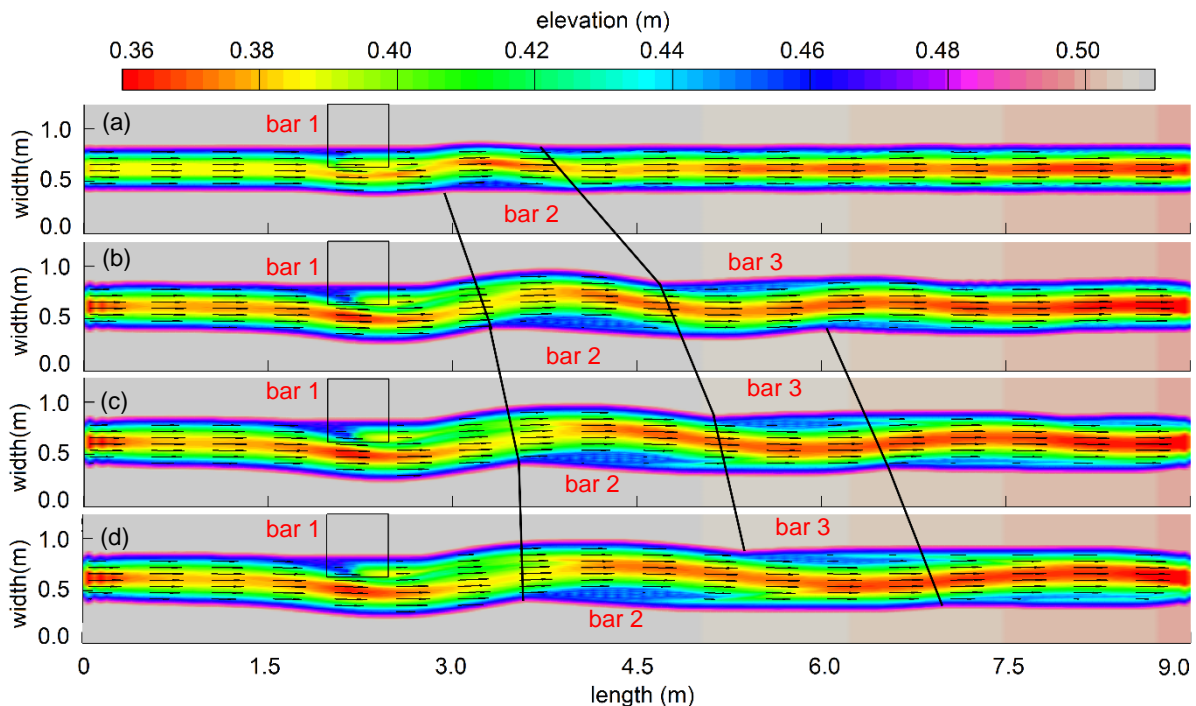
396

397 Figure 11. Adjusted channel patterns corresponding to different inflow conditions: (a) $1.5Q_{in}$; (b) comparison of
 398 adjusted bank lines for two different flow conditions, i.e. Q_{in} and $1.5Q_{in}$.

399 The above numerical experiments are conducted under the condition that the five vegetation
 400 zones are separated by equal distance. The meandering response of the channel form can be
 401 easily understood due to the location of vegetation zones. Herein, another numerical experiment
 402 with a single vegetation patch is designed and conducted. Figure 12 presents the resulting
 403 alluvial process in response to the single vegetation zone. The simulation results indicate that a
 404 single vegetation zone can also trigger the formation of a meandering channel with the maximum
 405 bank curvature located behind the vegetation zone. Channel widening occurs at the opposite
 406 side of the vegetation zone and the curve length becomes larger over time (line 1 shows the end
 407 of the first curve). The changes in velocity field around the vegetation lead to an oscillation in
 408 downstream velocity, causing the formation of a second curve after the vegetation; similarly, the
 409 curve width increases over time (as shown in line 2). Moreover, lateral bank erosion occurs along
 410 the whole downstream channel behind the vegetation zone. Although meandering occurs, it has
 411 a relative smaller intensity due to the weaker effects on flow caused by a single vegetation patch.
 412 Additionally a bar (bar 1 in Figure 12) is created at the location of the vegetation zone; following
 413 the meandering curve, a larger bar (bar 2) is formed due to the effects of upstream vegetation on
 414 channel erosion and deposition; the third and fourth bars appear and develop gradually along the

415 channel. It can be expected that the erosion and deposition patterns of a stream corridor become
 416 much more diverse and complicated over time if vegetation zones become more irregular.

417 The above hypothetical numerical experiments confirm that riparian and in-stream vegetation
 418 coves have a significant impact on local channel hydraulics and thereby stream morphology. The
 419 results imply that vegetation plays a key role in pushing flow towards the opposite side and
 420 hence protecting the localised bed; however it may cause severe erosion at the opposite side of
 421 the channel. The vegetation effects are persistent along the channel and further downstream,
 422 which may have a positive impact on and enhance stream biodiversity. This suggests that well-
 423 planned vegetation planting can be an effective natural approach for river restoration.



424

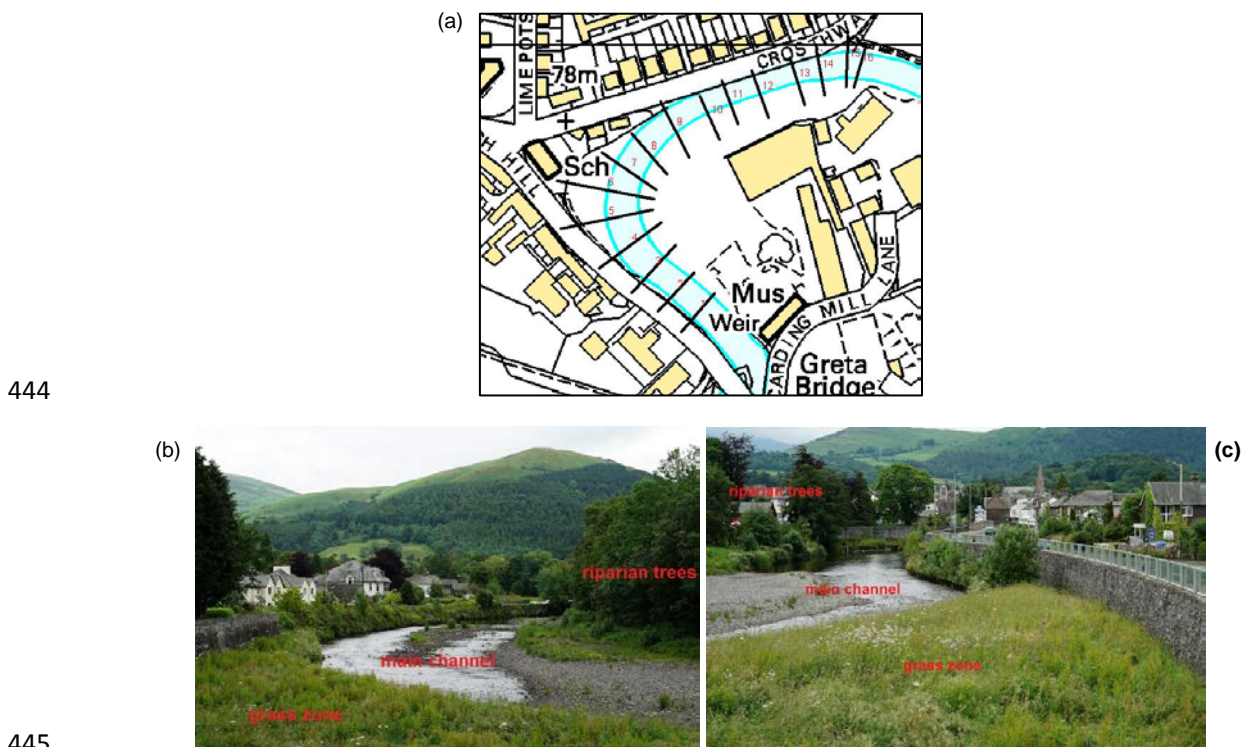
425 Figure 12. Channel pattern adjustment in response to a single vegetation zone under the condition of $1.5Q_{in}$

426 3.3. Morphological changes at a natural bend of River Creta

427 The capability and performance of the current model are further demonstrated and confirmed
 428 through application to a natural river reach. The study concerns a short reach of the River Greta
 429 located in Keswick, UK. The river reach is about 160 m long and has a varying width of 10 m to
 430 40 m, featuring a sharp bend. The difficulty in modelling morphological changes in a natural bend
 431 has been investigated in details by Guan et al. (2016) which did not account for the effects of
 432 vegetation, Field surveys show that the river channel is extensively covered by riparian

433 vegetation that may be separated into two zones, i.e. the grass area at the outer bank and the
 434 area at the inner bank of the river bend, as shown in Figure 13(a, b). During the flood periods,
 435 morphological changes regularly take place at the sharp bend and field survey data is available
 436 for this study.

437 Digital Terrain Models (DTMs) with a 1m x 1m resolution are reconstructed based on measured
 438 raw point data to represent the bed terrain of the site in August 2005 and July 2006, before and
 439 after the flooding period 2005-2006. The hydrograph of 15-minute intervals from January 2005 to
 440 July 2006 (Figure 14) is available at the Low Briery station, upstream of the study site. Most of
 441 the time, the flow discharge is smaller than 30 m³/s. Field surveys demonstrate that
 442 geomorphological changes are insignificant during the low flow period. Thus this study only
 443 focuses on flooding periods when flow is greater than 30 m³/s.



445

446

447

Figure. 13 The study river reach: (a) map showing the study site; (b) photo facing upstream; (c) photo facing downstream.

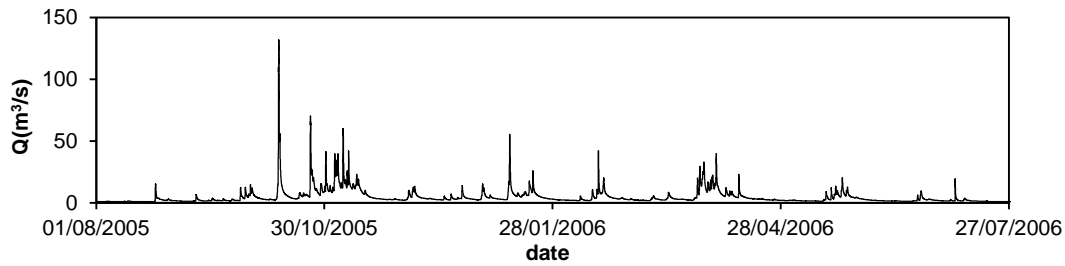


Figure 14. The inflow hydrograph recorded at the Low Briery gauge station

448

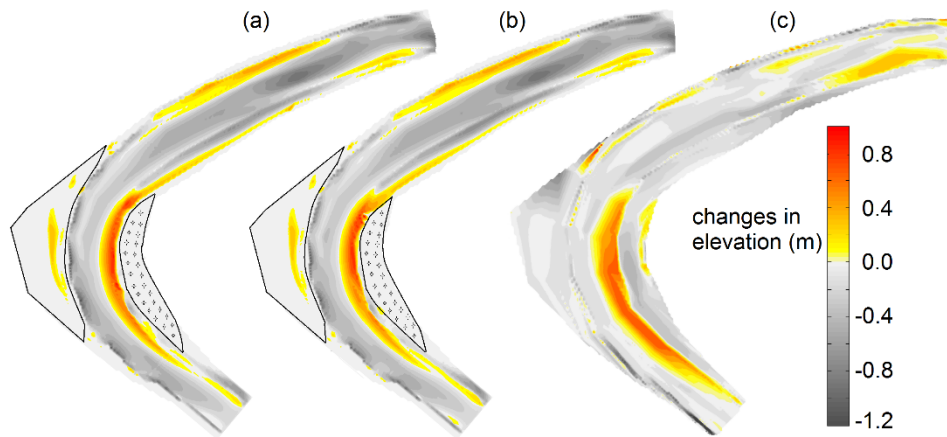
449

450 The study domain is discretised by a grid with uniform cells of $1\text{ m} \times 1\text{ m}$. The Manning's
 451 coefficient is set to 0.03 in the river channel and 0.035 in the grass zone. The drag coefficient C_d
 452 is assumed to be 2.0 for the emergent vegetation zone. The projected area λ is equal to 0.15 or
 453 0.25 in order to test the model sensitivity. Non-uniform sediment with diameters of 0.02 m (30%),
 454 0.04 m (40%), and 0.06 m (30%) is used and upstream inflow sediment load is neglected. The
 455 recorded flow discharge is used as the inflow boundary condition to drive flow in the study reach,
 456 and the corresponding stage-discharge curve is imposed at the outflow boundary. The radius of
 457 the bend is estimated to be 60 m and used in the simulations.

458 Figure 15 shows the predicted and measured changes in bed elevation at the bend during the
 459 multiple flood events from 2005 to 2006. Overall, the model predicts the formation of a bar, and
 460 both the location and pattern of the deposition bar at the bend agree reasonably well with
 461 measurements. Main deposition occurs at the inner bank of the bend. Small differences exist in
 462 the projected area. The model predicts a similar magnitude in the deposition depth, compared
 463 with the measured value. However, the model under-estimates the bar size; while in the main
 464 channel, it over-estimates the bed erosion.

465 Due to the spatial and temporal complexity of a natural study case and the scarcity of high-
 466 quality data, the simulation results are obtained without intensive model calibration. The
 467 simulation results may also be affected by the following uncertain factors; The time interval
 468 between the two DTMs representing the bed terrains before and after the flood is 1 year; the
 469 current simulation only considers the flooding periods with flow rates over $30\text{ m}^3/\text{s}$ and the
 470 recovery of channel morphology during low flow periods is neglected which inevitably leads to
 471 uncertainty. Sediment flux from upstream may significantly affect the hydro-geomorphology in the
 472 study reach but cannot be taken into account due to the lack of data. Moreover, accurate

473 parameterisation, such as sediment composition, viscosity and sediment transport capacity, is
 474 difficult, if not impossible, for a natural study case. Due to all these uncertainties linked to data
 475 scarcity, the simulation results are considered to be acceptable and the current model is
 476 demonstrated to be capable of predicting morphological changes during flooding over riparian
 477 vegetated channel in real cases.



478

479 Figure 15. Predicted and measured changes in bed elevation during the flooding periods from August 2005 to

480 July 2006: (a) $\lambda = 0.15$; (b) $\lambda = 0.25$; (c) the measured changes.

481

482 4. Conclusions

483 A two-dimensional model system has been developed and presented for simulating river
 484 hydraulics and morphology in the presence of various vegetation covers. The model system
 485 solves the full 2D shallow water equations and a non-equilibrium sediment transport equation,
 486 with a new module developed to consider the effects of both emergent and submerged
 487 vegetation. Also, the secondary flow effects have been incorporated into the 2D model system
 488 through the use of dispersion terms, leading to more accurate representation of river flow
 489 hydraulics.

490 The new model system has been validated against a number of laboratory-scale test cases,
 491 including flows over fixed and movable beds. The results show that both stream hydraulics and
 492 channel morphological changes in the presence of vegetation are reproduced reasonably well,
 493 with the bed elevation changes, bank retreat and thalweg meandering correctly captured.
 494 Numerical experiments are then designed and performed to investigate the adjustment of

495 channel patterns to riparian vegetation. Numerical predictions indicate that vegetation imposes
496 significant influence on flow dynamics by pushing the flow towards the opposite sides of the
497 vegetation zones, leading to excessive erosion. With multiple vegetation covers, the channel
498 tends to adjust itself to the meandering form. More complicated and irregular vegetation covers
499 may create diverse channel patterns, which may have important implications to biodiversity of the
500 local environment. Finally, the model's performance and capability are further demonstrated by
501 simulating a natural river bend and the simulation results indicate that the model is generally
502 capable of predicting river hydraulics, sediment transport and morphological changes during
503 flooding in a channel covered with vegetation. The model may therefore have great potential to
504 be used for a variety of applications in river engineering and management.

505

506 **Acknowledgements**

507 The authors would like to thank colleague Samantha Mahaffey from Newcastle University for
508 proof-reading the manuscript. Thanks also go to the Environment Agency for providing data for
509 the River Creta case study, which may be requested from [Inforequests.cmbinc@environment-](mailto:Inforequests.cmbinc@environment-agency.gov.uk)
510 [agency.gov.uk](mailto:Inforequests.cmbinc@environment-agency.gov.uk).

511

512 **References**

513 Abad, J.D., Buscaglia, G.C., Garcia, M.H., 2008. 2D stream hydrodynamic, sediment transport and
514 bed morphology model for engineering applications. *Hydrological Processes* 22(10) 1443-1459.

515 Alonso, C.V., 2004. Transport mechanics of stream-borne logs.

516 Anderson, B.G., Rutherford, I.D. and Western, A.W., 2006. An analysis of the influence of riparian
517 vegetation on the propagation of flood waves. *Environmental Modelling & Software*, 21(9) 1290-
518 1296.

519 Armanini, A., Cavedon, V., Righetti, M., 2010. Evaluation of the flow resistance in mobile bed
520 vegetated rivers, In: Dittrich, K., Aberle & Geisenhainer (Ed.), *River Flow 2010*: Braunschweig,
521 Gernany.

522 Baptist, M.J., Babovic, V., Uthurburu, J.R., Keijzer, M., Uittenbogaard, R.E., Mynett, A., Verwey, A.,

- 523 2007. On inducing equations for vegetation resistance. *Journal of Hydraulic Research* 45(4) 435-
524 450.
- 525 Begnudelli, L., Valiani, A., Sanders, B.F., 2010. A balanced treatment of secondary currents,
526 turbulence and dispersion in a depth-integrated hydrodynamic and bed deformation model for
527 channel bends. *Advances in Water Resources* 33(1) 17-33.
- 528 Bennett, S.J., Pirim, T., Barkdoll, B.D., 2002. Using simulated emergent vegetation to alter stream flow
529 direction within a straight experimental channel. *Geomorphology* 44(1–2) 115-126.
- 530 Bennett, S.J., Wu, W.M., Alonso, C.V., Wang, S.S.Y., 2008. Modeling fluvial response to in-stream
531 woody vegetation: implications for stream corridor restoration. *Earth Surface Processes and*
532 *Landforms* 33(6) 890-909.
- 533 Choi, S.-U., Kang, H., 2006. Numerical investigations of mean flow and turbulence structures of
534 partly-vegetated open-channel flows using the Reynolds stress model. *Journal of Hydraulic*
535 *Research* 44(2) 203-217.
- 536 Costabile, P. and Macchione, F., 2015. Enhancing river model set-up for 2-D dynamic flood modelling.
537 *Environmental Modelling & Software*, 67 89-107.
- 538 Cowan, W.L., 1956. Estimating hydraulic roughness coefficients. *Agricultural Engineering*(37) 473–
539 475.
- 540 Crosato, A., Saleh, M.S., 2011. Numerical study on the effects of floodplain vegetation on river
541 planform style. *Earth Surface Processes and Landforms* 36(6) 711-720.
- 542 Darby, S.E., 1999. Effect of riparian vegetation on flow resistance and flood potential. *Journal of*
543 *Hydraulic Engineering-ASCE* 125(5) 443-454.
- 544 De Vriend, H.J., 1977. A Mathematical Model Of Steady Flow In Curved Shallow Channels. *Journal of*
545 *Hydraulic Research* 15(1) 37-54.
- 546 Garcia, M.H., Lopez, F., Dunn, C., Alonso, C.V., 2004. Flow, turbulence, and resistance in a flume with
547 simulated vegetation.
- 548 Gorrick, S., Rodríguez, J.F., 2012. Sediment dynamics in a sand bed stream with riparian vegetation.
549 *Water Resources Research* 48(2).
- 550 Gran, K., Paola, C., 2001. Riparian vegetation controls on braided stream dynamics. *Water*
551 *Resources Research* 37(12) 3275-3283.
- 552 Green, J.C., 2005. Modelling flow resistance in vegetated streams: review and development of new

- 553 theory. *Hydrological Processes* 19(6) 1245-1259.
- 554 Guan, M., Wright, N., Sleight, P., 2013. A robust 2D shallow water model for solving flow over complex
555 topography using homogenous flux method. *International Journal for Numerical Methods in Fluids*
556 73(3) 225-249.
- 557 Guan, M., Wright, N., Sleight, P., 2014. 2D Process based morphodynamic model for flooding by
558 noncohesive dyke breach. *Journal of Hydraulic Engineering* 140(7).
- 559 Guan, M., Wright, N., Sleight, P., 2015a. Multimode morphodynamic model for sediment-laden flows
560 and geomorphic impacts. *Journal of Hydraulic Engineering* 141(6).
- 561 Guan, M., Wright, N.G., Sleight, P.A., Carrivick, J.L., 2015b. Assessment of hydro-morphodynamic
562 modelling and geomorphological impacts of a sediment-charged jökulhlaup, at Sólheimajökull,
563 Iceland. *Journal of Hydrology* 530 336-349.
- 564 Guan, M., Wright, N.G., Sleight, P.A., Ahilan, S. and Lamb, R., 2016. Physical complexity to model
565 morphological changes at a natural channel bend, *Water Resources Research* 52 6348–6364.
- 566 Guymer, I., 1998. Longitudinal Dispersion in Sinuous Channel with Changes in Shape. *Journal of*
567 *Hydraulic Engineering* 124(1) 33-40.
- 568 Hickin, E.J., 1984. Vegetation and river channel dynamics. *Canadian Geographer-Geographe*
569 *Canadien* 28(2) 111-126.
- 570 Hupp, C.R., Osterkamp, W.R., 1996. Riparian vegetation and fluvial geomorphic processes.
571 *Geomorphology* 14(4) 277-295.
- 572 Hou, J., Liang, Q., Zhang, H. and Hinkelmann, R., 2015. An efficient unstructured MUSCL scheme for
573 solving the 2D shallow water equations. *Environmental Modelling & Software*, 66 131-152.
- 574 James, C.S., Birkhead, A.L., Jordanova, A.A., O'Sullivan, J.J., 2004. Flow resistance of emergent
575 vegetation. *Journal of Hydraulic Research* 42(4) 390-398.
- 576 Jang, C.L., Shimizu, Y., 2007. Vegetation effects on the morphological behavior of alluvial channels.
577 *Journal of Hydraulic Research* 45(6) 763-772.
- 578 Jordanova, A.A., James, C.S., 2003. Experimental study of bed load transport through emergent
579 vegetation. *Journal of Hydraulic Engineering-ASCE* 129(6) 474-478.
- 580 Keller, E.A., Swanson, F.J., 1979. Effects of large organic material on channel form and fluvial
581 processes. *Earth Surface Processes and Landforms* 4(4) 361-380.
- 582 Li, S.S., Millar, R.G., 2011. A two-dimensional morphodynamic model of gravel-bed river with

- 583 floodplain vegetation. *Earth Surface Processes and Landforms* 36(2) 190-202.
- 584 Liang, Q.H., 2010. Flood Simulation Using a Well-Balanced Shallow Flow Model. *Journal of Hydraulic*
585 *Engineering-ASCE* 136(9) 669-675.
- 586 Lien, H., Hsieh, T., Yang, J., Yeh, K., 1999. Bend-Flow Simulation Using 2D Depth-Averaged Model.
587 *Journal of Hydraulic Engineering* 125(10) 1097-1108.
- 588 Lopez, F., Garcia, M.H., 2001. Mean flow and turbulence structure of open-channel flow through non-
589 emergent vegetation. *Journal of Hydraulic Engineering-ASCE* 127(5) 392-402.
- 590 Meyer-Peter, E., Müller, R., 1948. Formulas for bed load transport, Proc., 2nd Meeting: Stockholm,
591 Sweden, pp. 39–64.
- 592 Morin, J., Leclerc, M., Secretan, Y., Boudreau, P., 2000. Integrated two-dimensional macrophytes-
593 hydrodynamic modeling. *Journal of Hydraulic Research* 38(3) 163-172.
- 594 Odgaard, A., 1986. Meander Flow Model. I: Development. *Journal of Hydraulic Engineering* 112(12)
595 1117-1135.
- 596 Pasche, E., Rouvé, G., 1985. Overbank flow with vegetatively roughened floodplains. *Journal of*
597 *Hydraulic Engineering* 111(9) 1262-1278.
- 598 Sellin, R.H.J., Bryant, T.B., Loveless, J.H., 2003. An improved method for roughening floodplains on
599 physical river models. *Journal of Hydraulic Research* 41(1) 3-14.
- 600 Song, C.G., Seo, I.W., Kim, Y.D., 2012. Analysis of secondary current effect in the modeling of shallow
601 flow in open channels. *Advances in Water Resources* 41(0) 29-48.
- 602 Soulsby, R., 1997. Dynamics of marine sands: a manual for practical applications. Thomas Telford,
603 London, UK.
- 604 Stone, B.M., Shen, H.T., 2002. Hydraulic resistance of flow in channels with cylindrical roughness.
605 *Journal of Hydraulic Engineering-ASCE* 128(5) 500-506.
- 606 Tal, M., Paola, C., 2007. Dynamic single-thread channels maintained by the interaction of flow and
607 vegetation. *Geology* 35(4) 347-350.
- 608 Tal, M., Paola, C., 2010. Effects of vegetation on channel morphodynamics: results and insights from
609 laboratory experiments. *Earth Surface Processes and Landforms* 35(9) 1014-1028.
- 610 Temple, D.M., 1986. Velocity distribution coefficients for grass-lined channels. *Journal of Hydraulic*
611 *Engineering-ASCE* 112(3) 193-205.
- 612 Tsujimoto, T., 1999. Fluvial processes in streams with vegetation. *Journal of Hydraulic Research* 37(6)

- 613 789-803.
- 614 Vacondio, R., Dal Palù, A. and Mignosa, P., 2014. GPU-enhanced Finite Volume Shallow Water solver
615 for fast flood simulations. *Environmental Modelling & Software*, 57 60-75.
- 616 Vionnet, C.A., Tassi, P.A., Martin Vide, J.P., 2004. Estimates of flow resistance and eddy viscosity
617 coefficients for 2D modelling on vegetated floodplains. *Hydrological Processes* 18(15) 2907-2926.
- 618 Wu, F.C., Shen, H.W., Chou, Y.J., 1999. Variation of roughness coefficients for unsubmerged and
619 submerged vegetation. *Journal of Hydraulic Engineering-ASCE* 125(9) 934-942.
- 620 Wu, W., 2004. Depth-averaged two-dimensional numerical modeling of unsteady flow and nonuniform
621 sediment transport in open channels. *Journal of Hydraulic Engineering-ASCE* 130(10) 1013-1024.
- 622 Wu, W., Shields, F.D., Bennett, S.J., Wang, S.S.Y., 2005a. A depth-averaged two-dimensional model
623 for flow, sediment transport, and bed topography in curved channels with riparian vegetation.
624 *Water Resources Research* 41(3) W03015.
- 625 Wu, W.M., Shields, F.D., Bennett, S.J., Wang, S.S.Y., 2005b. A depth-averaged two-dimensional
626 model for flow, sediment transport, and bed topography in curved channels with riparian
627 vegetation. *Water Resources Research* 41(3).
- 628